Atmospheric
Chemistry
and Physics

A new balance formula to estimate new particle formation rate: reevaluating the effect of coagulation scavenging

Runlong Cai and Jingkun Jiang

State Key Joint Laboratory of Environmental Simulation and Pollution Control, School of Environment,
Tsinghua University, Beijing 100084, China

Correspondence to: Jingkun Jiang (jiangjk@tsinghua.edu.cn)

Abstract. A new balance formula to estimate new particle formation rate is proposed. It is derived from the aerosol general dynamic equation in the discrete form and then converted into an approximately continuous form for analyzing data from new particle formation (NPF) field campaigns. The new formula corrects the underestimation of the coagulation scavenging effect that occurred in the previously used formulae. It also clarifies the criteria for determining the upper size bound in measured aerosol size distributions for estimating new particle formation rate. An NPF field campaign was carried out from 7 March to 7 April 2016 in urban Beijing, and a diethylene glycol scanning mobility particle spectrometer equipped with a miniature cylindrical differential mobility analyzer was used to measure aerosol size distributions down to ∼ 1 nm. Eleven typical NPF events were observed during this period. Measured aerosol size distributions from 1 nm to 10 μm were used to test the new formula and the formulae widely used in the literature. The previously used formulae that perform well in a relatively clean atmosphere in which nucleation intensity is not strong were found to underestimate the comparatively high new particle formation rate in urban Beijing because of their underestimation or neglect of the coagulation scavenging effect. The coagulation sink term is the governing component of the estimated formation rate in the observed NPF events in Beijing, and coagulation among newly formed particles contributes a large fraction to the coagulation sink term. Previously reported formation rates in Beijing and in other locations with intense NPF events might be underestimated because the coagulation scavenging effect was not fully considered; e.g., estimated formation rates of 1.5 nm particles in this campaign using the new formula are

1.3–4.3 times those estimated using the formula neglecting coagulation among particles in the nucleation mode.

1 Introduction

New particle formation (NPF) is a frequently occurring phenomenon in the atmospheric environment. In a typical NPF event, gaseous precursors burst out into particles due to nucleation and lead to a rapid increase in the atmospheric aerosol population. Nucleated particles can grow quickly to increase the number concentration of cloud condensation nuclei (Kerminen et al., 2012; Kuang et al., 2009; Leng et al., 2014) and thus have indirect impacts on radiative forcing and global climate (Lohmann and Feichter, 2005). The continuous growth of nucleated particles also provides increasing aerosol surface area for heterogeneous physicochemical processes. NPF studies can trace back to the early 20th century (Aitken, 1911), and NPF events have been observed in various atmospheric environments, e.g., from the city to the countryside, from desert (Misaki, 1964) to rain forest (Zhou et al., 2002), from the continent to the ocean (Covert et al., 1992), from the Equator (Clarke et al., 1998) to polar areas (Covert et al., 1996; Park et al., 2004), and from the troposphere to the stratosphere (Lee et al., 2003).

The formation rate at which the growth flux passes a certain diameter is a key parameter to quantitatively describe NPF events. Different formulae have been used to estimate new particle formation rate from measured aerosol size distributions, and they mainly originate from two approaches. One is from the definition of nucleation rate (Heisler and Friedlander, 1977; Weber et al., 1996) and the other is a pop-

ulation balance method (Kulmala et al., 2001, 2012). The consistency of these two approaches was tested using a numerically simulated NPF event, and a relative error of less than 20 % was reported (Vuollekoski et al., 2012). The simulated NPF event had a maximum formation rate of less than $1 \, \text{cm}^{-3} \, \text{s}^{-1}$. However, the reported formation rates in the atmosphere vary on a large scale, e.g., from approximately 10^{-2} to $10^4 \, \text{cm}^{-3} \, \text{s}^{-1}$ (Kulmala et al., 2004). Because of the assumptions made in these two approaches, their validity in describing NPF events with a high formation rate needs to be further explored. A high fraction of newly formed particles is scavenged by coagulation before they grow into larger sizes. Both approaches potentially underestimate the contribution of the coagulation scavenging effect when calculating the formation rate from measurement data. They perform well only in clean atmospheric environments in which nucleation intensity is not strong and aerosol concentration is relatively low; i.e., the coagulation scavenging effect is less important.

The effect of coagulation scavenging is more prominent when estimating the formation rate of sub-3 nm particles because of their high diffusivities and high concentrations during NPF events. Due to instrument limitations, aerosol size distributions of sub-3 nm particles were not available in many previous NPF field campaigns. Recent developments in diethylene glycol (DEG) condensation particle counters (CPCs; Iida et al., 2009; Vanhanen et al., 2011) have made it feasible to develop new scanning mobility particle spectrometers (SMPSs) for extending aerosol size distribution measurement from ∼3 nm down to ∼1 nm (Jiang et al., 2011a; Franchin et al., 2016). These new spectrometers were deployed in atmospheric observations (Jiang et al., 2011b) and in chamber measurements (Franchin et al., 2016) to study NPF. A miniature cylindrical differential mobility analyzer (mini-cyDMA; Cai et al., 2017) was developed to improve the performance of the DEG-SMPS.

In many locations in China, high emissions lead to both high concentrations of gaseous precursors and high atmospheric aerosol concentrations. NPF has frequently been observed, even in megacities such as Beijing and Shanghai (Wu et al., 2007; Kulmala et al., 2016; Wang et al., 2017). In most previous studies, the above population balance method was used to estimate new particle formation rates in China. The reported formation rates of 3 nm particles and larger ones are typically in the range of 1–$10 \, \text{cm}^{-3} \, \text{s}^{-1}$ (Wang et al., 2013; Leng et al., 2014; An et al., 2015; Qi et al., 2015). One study in Shanghai reported a rate of 112.4 to $271.0 \, \text{cm}^{-3} \, \text{s}^{-1}$ for the formation of 1.5 nm particles inferred from a DEG-CPC (Xiao et al., 2015). For these intense NPF events, the above balance approach may underestimate the coagulation scavenging effect and thus lead to underestimation in the reported formation rate. In addition, applying new SMPSs to measure aerosol size distributions down to ∼1 nm will help to better quantify the formation rate and its governing factors in typical locations in China.

To estimate new particle formation rates, various particle size ranges were used in previous formulae. The definition approach tries to limit the size range towards the minimum detected diameter (Kuang et al., 2008; Weber et al., 1996), while studies with the population balance method have used various size ranges. Some studies used the aerosol size distributions from the minimum detected diameter up to 25 nm (Kulmala et al., 2001; Dal Maso et al., 2005; Wu et al., 2007; Wang et al., 2013). Kulmala et al. (2004) recommended the upper size bound as the maximum size that the critical cluster can reach during a short time interval of growth. There are also studies using narrower size ranges, such as from 3 to 6 nm (Sihto et al., 2006; Paasonen et al., 2009; Wang et al., 2011; Vuollekoski et al., 2012) and from 1.34 to 3 nm (Xiao et al., 2015). In principle, the estimated formation rates may vary when different particle size ranges are used. Assumptions made while deriving these formulae should be fully considered when proposing criteria to choose the particle size range.

In this study, a new population balance formula for estimating the new particle formation rate was derived from the aerosol general dynamic equation to properly account for the effect of coagulation scavenging, especially for analyzing intense NPF events. An NPF field campaign was carried out in Beijing. Aerosol size distributions down to ∼1 nm were measured using the DEG-SMPS equipped with the mini-cyDMA. Data from this campaign and from the literature are used to test the new formula and other widely used formulae. Different formulae are compared and their applicability in analyzing intense NPF events is addressed. Criteria to choose the particle size range for formation rate estimation are proposed and evaluated. The governing components of the new formation rate in Beijing are discussed and compared to those from other locations in the world.

2 Theory

2.1 The new balance formula to estimate formation rate

The new formula, which is based on the definition of droplet current and the aerosol general dynamic equation (see Appendix A for its derivation), is shown in Eq. (1):

$$
I = \frac{\mathrm{d}N_{[d_k, d_u)}}{\mathrm{d}t} + \sum_{d_g = d_k}^{d_{u-1}} \sum_{d_i = d_{\min}}^{+\infty} \beta_{(i,g)} N_{[d_i, d_{i+1})} N_{[d_g, d_{g+1})}
$$
$$
- \frac{1}{2} \sum_{d_g = d_{\min}}^{d_{u-1}} \sum_{d_i^3 = \max(d_{\min}^3, d_k^3 - d_{\min}^3)}^{d_{i+1}^3 + d_{g+1}^3 \leq d_u^3} \beta_{(i,g)} N_{[d_i, d_{i+1})} N_{[d_g, d_{g+1})}
$$
$$
+ n_u \cdot \mathrm{GR}_u, \tag{1}
$$

where J_k is the formation rate of particles at size d_k, N is the particle number concentration, and $N_{[d_k, d_u)}$ is defined as the
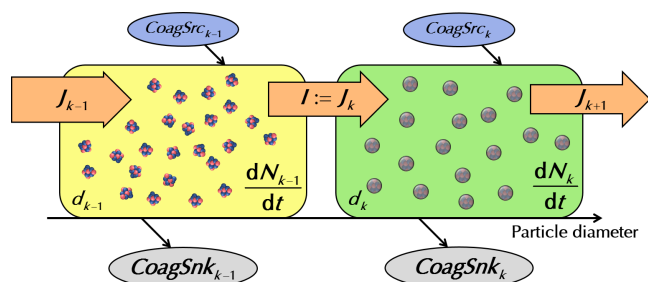
Figure 1. Schematic of the general dynamic equation.

total number concentration of particles in the size range from d_k to d_u (particles with diameters of d_u are not accounted for); d_i refers to the lower bound of each measured size bin; $\beta_{(i,g)}$ is the coagulation coefficient when particles with the diameter d_i collide with particles with the diameter d_g; n is the particle size distribution function that equals $\mathrm{d}N\,/\,\mathrm{d}d_p$; GR_u is the particle growth rate at d_u, i.e., $\mathrm{d}d_u\,/\,\mathrm{d}t$; and d_u is the upper bound of the size range for calculation. The size of the minimum cluster in theory and the lowest size limit of the measuring instrument in practice is represented by $d_{\min}$. The last three terms on the right-hand side (RHS) of Eq. (1) are the coagulation sink term (CoagSnk), the coagulation source term (CoagSrc), and the condensational growth term.

The two assumptions of Eq. (1) are that (a) transport, dilution, primary emissions, and other losses except for coagulation loss in the size range from d_k to d_u are comparatively negligible, and (b) when deriving the fourth term on the RHS of Eq. (1), the net coagulation (net result of both formation and scavenging due to coagulation) of any particle larger than d_u with other particles is negligible. These two assumptions are also the criteria to determine d_u. The mathematical expression of population balance in Eq. (1) in the discrete form is illustrated by Fig. 1. The time rate of change of particles at d_k is equal to source minus sink. Source values are the condensational flux into d_k (J_k) and formation due to coagulation among smaller particles or clusters (CoagSrc$_k$). Sink values are the condensational flux out of d_k (J_{k+1}) and scavenging due to coagulation with other particles or clusters (CoagSnk$_k$). Nucleation rate, I, is defined as J_k when d_k is the size of the critical cluster (nuclei). Equation (1) is obtained by adding these single population balance equations from d_k to d_u, converting it from the discrete form into the continuous form, and approximating J_u with the product of measured n_u and GR_u. Note that Eq. (1) is still an approximate formula for particle formation rate because CoagSnk and CoagSrc are calculated by using size bins and the coagulation effect of particles smaller than $d_{\min}$ is not accounted for. For rigorous mathematical derivation and detailed illustration, please refer to Appendix A.

2.2 Previous approaches to estimate formation rate

The population balance method proposed in previous studies is shown in Eq. (2) (Kulmala et al., 2001, 2012):

$$J_k = \frac{\mathrm{d}N_{[d_k,d_u)}}{\mathrm{d}t} + \mathrm{CoagS}_m \cdot N_{[d_k,d_u)} + \frac{N_{[d_k,d_u)}}{(d_u - d_k)} \cdot \mathrm{GR}_{[d_k,d_u)}, \quad (2)$$

where coagulation sink, CoagS_m, is defined as in Eq. (3).

$$\mathrm{CoagS}_m = \int_0^{+\infty} \beta_{(i,m)} n_i \,\mathrm{d}d_i \quad (3)$$

The subscript m corresponds to the representing diameter, d_m, for particles ranged from d_k to d_u; d_m is often estimated as the geometric mean diameter of d_k and d_u. Equations (1) and (2) look similar because they are both derived from the general dynamic equation, while their detailed differences are illustrated in Appendix B.

The definition approach to calculate new particle formation rate is shown in Eq. (4) (Heisler and Friedlander, 1977; Weber et al., 1996; Iida et al., 2006; Kuang et al., 2008, 2012).

$$J_k = n_k \cdot \mathrm{GR}_k \quad (4)$$

Equation (4) focuses on the flux into d_k and is theoretically correct in the continuous space of particle diameter. However, when applying Eq. (4) in practice, the size distribution of particles smaller than d_k is required, which is difficult to obtain (See Appendix B). Usually diameter bins larger than d_k are used to estimate the particle formation rate when using the practical expression of Eq. (4) (e.g., Eq. 9 as defined in Sect. 4.3). As illustrated in Fig. 1, such approximation essentially neglects the first three terms on the RHS of Eq. (1) and may lead to underestimation of the particle formation rate because of neglecting the coagulation scavenging effect, especially when intense NPF events are analyzed.

2.3 Previous formulae for comparison

Equation (5) is a widely used balance formula to estimate the formation rate in previous studies (Kulmala et al., 2001; Dal Maso et al., 2005; Wu et al., 2007; Shen et al., 2011; Wang et al., 2013):

$$J_{1.5} = \frac{\mathrm{d}N_{[1.5,25)}}{\mathrm{d}t} + N_{[1.5,25)} \sum_{d_i=1.5\,\mathrm{nm}}^{+\infty} \beta_{(i,8)} N_i$$

$$+ \frac{N_{[1.5,25)}}{(25 - 1.5)\ \mathrm{nm}} \cdot \mathrm{GR}_{[1.5,25)}, \quad (5)$$

where N_i is the number concentration of size bin i. Corresponding to Eq. (2), d_u is 25 nm and d_m is 8 nm in Eq. (5). By comparing Eq. (5) with Eq. (1), it can be concluded that Eq. (5) estimates CoagSnk using a representative CoagS_m and neglects CoagSrc. The growth rates in all formulae in

Sect. 2.2 were estimated using the mode-fitting method suggested in Kulmala et al. (2012).

When calculating $CoagS_m$, particles smaller than d_m (Kulmala et al., 2012) or even d_u are neglected in some previous studies. The corresponding formulae are shown in Eqs. (6) and (7). The only difference among Eqs. (5), (6), and (7) is the lower bound when calculating $CoagS_m$ in the second term on the RHS of these equations.

$$J_{1.5} = \frac{dN_{[1.5,25)}}{dt} + N_{[1.5,25)} \sum_{d_i=8\,\mathrm{nm}}^{+\infty} \beta_{(i,8)} N_i$$
$$+ \frac{N_{[1.5,25)}}{(25-1.5)\,\mathrm{nm}} \cdot GR_{[1.5,25)} \tag{6}$$

$$J_{1.5} = \frac{dN_{[1.5,25)}}{dt} + N_{[1.5,25)} \sum_{d_i=25\,\mathrm{nm}}^{+\infty} \beta_{(i,8)} N_i$$
$$+ \frac{N_{[1.5,25)}}{(25-1.5)\,\mathrm{nm}} \cdot GR_{[1.5,25)} \tag{7}$$

The upper bound, d_u, is selected as 6 nm is some recent studies (Sihto et al., 2006; Riipinen et al., 2007; Paasonen et al., 2009; Wang et al., 2011; Vuollekoski et al., 2012; Wang et al., 2015) as shown in Eq. (8).

$$J_{1.5} = \frac{dN_{[1.5,6)}}{dt} + N_{[1.5,6)} \sum_{d_i=1.5\,\mathrm{nm}}^{+\infty} \beta_{(i,3)} N_i$$
$$+ \frac{N_{[1.5,6)}}{(6-1.5)\,\mathrm{nm}} \cdot GR_{[1.5,6)} \tag{8}$$

It should be clarified that d_k in Eqs. (5)–(8) was usually 3 nm in previous studies due to the absence of sub-3 nm particle size distributions, and d_m in Eq. (8) was 4 nm rather than 3 nm in previous studies because 4 nm is almost the geometrical mean diameter of 3 and 6 nm. Particles smaller than 6 nm were neglected when estimating the coagulation sink term in some studies, although its uncertainties will not be discussed here. The expression of the condensational growth term, i.e., the third term on the RHS of Eq. (8), varies among studies; however, it does not influence the generality of the following discussion.

In previous studies, several size bins larger that d_k, typically 3 nm, were adopted when using the practical formula of the definition approach (Weber et al., 1996; Kuang et al., 2008), while here the size range from 1.5 to 2.5 nm is applied to estimate $J_{1.5}$ as shown in Eq. (9).

$$J_{1.5} = \frac{N_{[1.5,2.5)}}{(2.5-1.5)\,\mathrm{nm}} \cdot GR_{[1.5,2.5)} \tag{9}$$

3   Experiment

An NPF field campaign was carried out in Beijing. The observation period was from 7 March to 7 April 2016. The monitoring site is located on the top floor of a four-storey building in the center of the campus of Tsinghua University. Tsinghua is situated in the northwestern urban area of Beijing and the fourth-ring road is ~ 2 km to the south of the monitoring site. The site has been a $PM_{2.5}$ monitoring station since 1999 (He et al., 2001; Cao et al., 2014) and there are no tall buildings nearby. Potential pollution sources in the area are the three cafeterias on campus, which may produce cooking aerosol during meal times, located ~ 170 m to the northeast, ~ 170 m to the north, and ~ 350 m to the northwest.

A DEG-SMPS equipped with a mini-cyDMA specially designed for the classification of sub-3 nm particles was deployed to measure particles in the size range of 1–5 nm (Cai et al., 2017). A particle size distribution system, including an SMPS with a TSI nano-DMA, an SMPS with a TSI long DMA, and an aerodynamic particle sizer, was used to measure particles in the size range of 3 nm to 10 µm in parallel (Liu et al., 2016). Other instruments that produced data not used in this analysis are not listed here.

A C++ program was used to invert the particle size distribution from raw counts while incorporating diffusion losses inside the sampling tube, diffusion losses and charging efficiencies of the bipolar neutralizers, penetration efficiencies and transfer functions of DMAs, and detection efficiencies of CPCs (Hagen and Alofs, 1983; Jiang et al., 2011a). The particle density was assumed to be $1.6\,\mathrm{g\,cm^{-3}}$ according to local observation results (Hu et al., 2012). The mass accommodation coefficient was assumed to be 1.0, and temperature was assumed to be constant at 285 K, the average temperature during the observation period.

4   Results and discussion

4.1   Upper size bound for formation rate calculation

New particle formation rates using different upper size bounds, d_u, of 3, 6, 10, and 25 nm were calculated. Since the maximum size that new particles formed by nucleation have reached varies with time, the upper size bound should not be a constant value to minimize the interference of background particles. A varying upper size bound, d_b, was visually determined as the largest size bin in the size range from 3 to 25 nm with a frequency density (particle size distribution), $dN / \mathrm{dlog}d_p$, larger than 2.8×10^4 no. $\mathrm{cm^{-3}}$. Here 28 000 was determined visually according to the measured intensity plot of particle size distributions as an approximate boundary for newly formed particles and background particles. The value should be campaign specific or even event specific. Figure 2a indicates that d_b is almost the boundary for particles formed due to nucleation. Estimated $J_{1.5}$ using 2.0×10^4 no. $\mathrm{cm^{-3}}$ as the boundary differed little from that using 2.8×10^4 no. $\mathrm{cm^{-3}}$, indicating that the estimated $J_{1.5}$ is insensitive to the value for the boundary. It is reasonable to regard d_b as a relatively credible value when compared to others. Note that when using d_b as the upper size bound, the
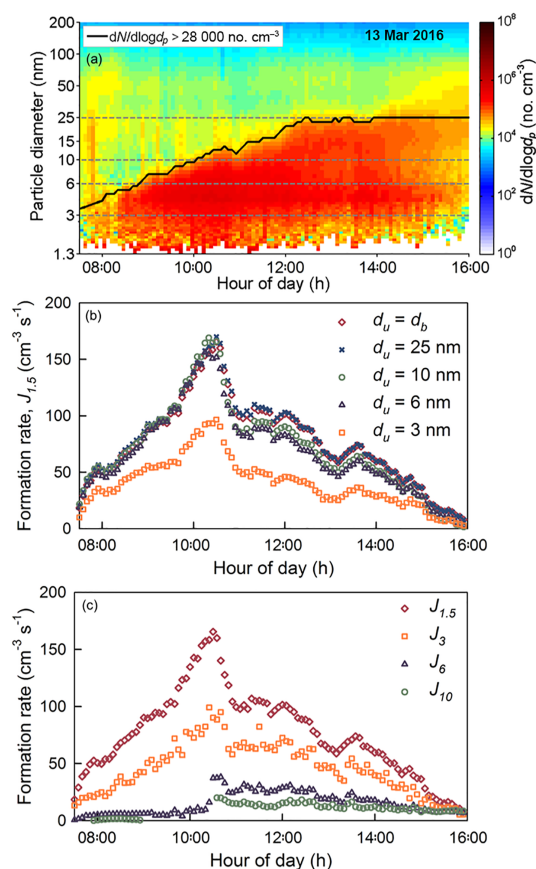
Figure 2. Comparison of formation rates estimated using different upper bounds, d_u. **(a)** A typical new particle formation event. Dashed gray lines represent different d_u values in Eq. (1). Solid black lines corresponds to d_b, i.e., the varying upper bound determined by $dN/d\log d_p$. **(b)** Estimated formation rates with different upper bounds, d_u, using Eq. (1). **(c)** Estimated formation rates with different d_k values using Eq. (1); d_u equals 25 nm and $d_{\min}$ equals 1.3 nm in the four scatter plots.

dN / dt term of newly formed particles in Eq. (1) is approximated by that of sub-25 nm particles to avoid the potential influence of varying size range on particle number concentration.

As shown in Fig 2b, estimated $J_{1.5}$ values using d_b and a constant value of 25 nm as the upper bounds are almost the same (the mean relative error is 2.2 %). The maximum difference between these two choices is ∼ 10 %, which appears before 08:00 when d_b is less than 5 nm and the number concentration of sub-25 nm particles is ∼ 2 times that of sub-6 nm particles and ∼ 3 that times of sub-3 nm particles. This indicates that the influence of non-freshly nucleated particles in estimating $J_{1.5}$ is not important because of their comparatively low diffusivities even though their concentration is comparatively high at the beginning of NPF events. Estimated $J_{1.5}$ values using d_u of 6 and 10 nm are in good consistency with those using d_b before 10:00 (the mean relative errors are 4.8 and 2.6 %, respectively). However, when particles formed by nucleation grow beyond the upper size bound, calculated $J_{1.5}$ is underestimated when using 6 and 10 nm as the upper bound. For example, the mean relative errors of estimated $J_{1.5}$ using d_u values of 6 and 10 nm between 10:30 and 15:00 are 18.6 and 12.8 %, respectively. When calculating $J_{1.5}$ using 3 nm as d_u, an average 47 % underestimation was found for this event.

The reason for underestimation when using smaller d_u can be illustrated by Fig. 2c. J_u is estimated by $n_u \cdot GR_u$ in Eq. (1). This estimation may be not accurate when d_u is small because the assumption that the net coagulation between any particle larger than d_u and other particles is negligible may be violated. As illustrated in the derivation of Eq. (1) in Appendix A, a nearly zero J_u is preferred when using Eq. (1). However, as shown in Fig. 2c, estimated J_3 is still a large fraction compared to $J_{1.5}$, while J_6 and J_{10} are 27.8 and 17.6 % of $J_{1.5}$ on average between 10:30 and 15:00, respectively. Although J_u is approximated by $n_u \cdot GR_u$ rather than simply neglected, this approximation may still lead to uncertainties.

Since $J_{1.5}$ values estimated from the varying d_b and a constant value of 25 nm are almost the same with an acceptable relative error even under the interference of non-freshly nucleated particles, 25 nm was adopted as the upper bound for calculating J in this study. It is reasonable to neglect J_u for simplicity when d_u is determined according to the two criteria. It should be clarified that 25 nm is not necessarily valid for all other studies because the upper bound should be determined by the two criteria and can be campaign specific. However, it can be concluded that a very small upper bound, such as 3 nm, is not recommended because particles formed by nucleation surely grow larger than 3 nm in a typical NPF event, while the intense primary emission of particles around 3 nm is rarely observed in the atmosphere (unless near the emission sources).

4.2 Comparison with previous formulae

Estimated $J_{1.5}$ values using Eqs. (1) and (5)–(9) on 13 March are shown in Fig. 3, and d_k, d_u, and $d_{\min}$ are 1.5, 25, and 1.3 nm, respectively, when using Eq. (1). It can be concluded that except for Eq. (8), other formulae significantly underestimate $J_{1.5}$ compared to Eq. (1). By comparing the contribution of each term on the RHS of Eqs. (1) and (5)–(9), it was found that the underestimation of formation rates is mainly caused by the underestimation of CoagSnk. Equation (9) simply neglects CoagSnk and other terms (dN / dt and CoagSrc) compared to Eq. (1), so its result is the lowest among the six formulae. Equation (5) estimates CoagSnk using an average $CoagS_m$, which leads to underestimation because CoagS at 8 nm happens to be smaller than at most other diameters in the size range from 1.5 to 25 nm, as illustrated in Appendix B. Equations (6) and (7) neglect particles smaller than 8 and 25 nm, respectively, when $CoagS_m$
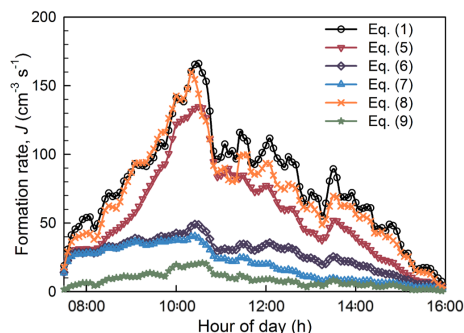
Figure 3. Comparison of formation rates estimated by different formulae.

Figure 4. (a) CoagSnk as a function of d_p, where d_p is the accounted minimum diameter when calculating CoagS_g for particles at all different d_g values, and scavenging due to coagulation with particles smaller than d_p is neglected, as defined by the formula in panel **(a)**. The dashed line corresponding to CoagSnk on a non-NPF day is also monotonously decreasing with the increase in d_{min} by a negligible slope. **(b)** Time evolution of CoagSnk versus time on an NPF day (13 March) and a non-NPF day (12 March); d_p is defined the same as in panel **(a)**. N is the number concentration of particles in the size range from 1.5 to 25 nm, while $\text{CoagS}_{8\,\text{nm}}$ is calculated using Eq. (3).

is calculated. Such a simplification may be reasonable for a relatively clean atmosphere in which nucleation intensity is not strong; however, these approximations are not suitable for analyzing typical NPF events in Beijing during which coagulation among nucleation mode particles is a major proportion of CoagSnk. $J_{1.5}$ estimated using Eq. (8) agrees well with that estimated using Eq. (1); however, it does not mean that 6 nm serves as a better upper size bound than 25 nm. The agreement between the results estimated using Eqs. (1) and (8) is due to the more accurate estimation of CoagSnk when using an average CoagS_m in a narrower size range. In addition, in this case the underestimation of CoagSnk when using Eq. (8) is coincidently canceled out by the overestimation of the formation rate caused by neglecting CoagSrc.

The importance of coagulation scavenging among newly formed particles due to nucleation is illustrated in Fig. 4. Scavenging due to coagulation with particles smaller than d_p is neglected, as mathematically defined in the formula in Fig. 4a. CoagSnk increases rapidly with the decrease in d_p rather than maintaining an approximately constant value during NPF events, indicating that coagulation among nucleated particles contributes a considerable fraction to CoagSnk in Beijing. The necessity of a sub-3 nm particle size distribution is also demonstrated, which means that estimated J_3 may also be underestimated due to the absence of sub-3 nm data, as illustrated in Appendix B. Approximation of CoagSnk estimated using a representative CoagS_m is also shown in Fig. 4b, indicating the underestimation of the new particle formation rate when applying Eq. (5) to analyze NPF events in Beijing. However, calculated CoagSnk on a non-NPF event day and in non-NPF periods on NPF days is almost unaffected by the coagulation scavenging effect of particles in nucleation mode (smaller than 25 nm) because the number concentration of nucleation mode particles at non-NPF times is comparatively low.
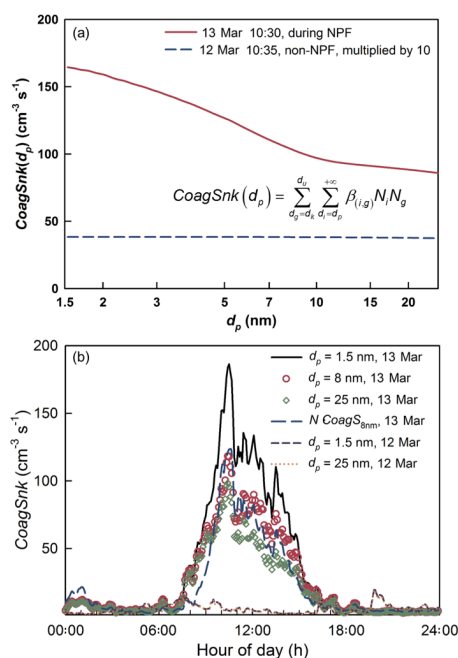
4.3 Characteristics of estimated formation rate in Beijing

For the NPF events observed in the Beijing campaign, CoagSnk is a governing component of the estimated $J_{1.5}$. The estimated formation rate on 13 March and the four terms on the RHS of Eq. (1), i.e., dN/dt, CoagSnk, CoagSrc, and the condensational growth term, are shown in Fig. 5. CoagSnk is almost the same as the estimated $J_{1.5}$ in Beijing, while the difference between them is mainly due to dN/dt with an absolute value that is comparatively higher at the beginning and the end of the NPF event. The condensational growth term, $n_u \cdot \text{GR}_u$, is negligible compared to other terms, which is reasonable since J_u is assumed to be unimportant when determining d_u in Eq. (1). The governing role of CoagSnk in estimated formation rates in Beijing emphasizes the importance of fully considering the coagulation scavenging effect among particles formed by nucleation. Equations (5)–(9) may fit well in relatively clean atmospheric environments in which the new particle formation rate is comparatively low, such as in Hyytiälä, and the agreement of Eqs. (8) and (9)
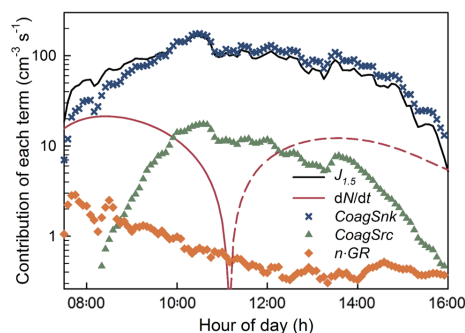
Figure 5. Contribution of each term to the estimated formation rate; dN/dt is obtained by fitting and shown as an absolute value with solid and dashed lines corresponding to positive and negative parts, respectively. Note that the upper bound, d_u, equals d_b as defined in Sect. 4.1 for better accuracy; however, it does not affect the generality of the result.

has been reported in a numerically simulated NPF event in which J_3 is less than $1\,\mathrm{cm^{-3}\,s^{-1}}$ (Vuollekoski et al., 2012). However, problems appear when applying them in urban Beijing because of underestimating the governing fraction of estimated $J_{1.5}$, i.e., CoagSnk.

Coagulation sink, CoagS, is not the major reason for the governing role of CoagSnk in Beijing. It is generally considered that the atmosphere in a typical urban area in China, such as Beijing, is comparatively polluted. However, observed NPF events mainly occur on clean days when the air mass comes from the north or northwest of Beijing. The mean $PM_{2.5}$ mass concentration reported by the nearest national monitoring station, Wanliu station, was $10.4\,\mu g\,cm^{-3}$ during all NPF events in this campaign. The aerosol surface area concentration is characterized by the Fuchs surface area, A_{Fuchs} (McMurry, 1983), and the condensation sink, CS (Kulmala et al., 2001), which are often used to examine the coagulation scavenging effect. The positive correlation between A_{Fuchs} and CS is illustrated in McMurry et al. (2005), while CS can be regarded as the CoagS of sulfuric acid molecules. Figure 6a shows the comparison of A_{Fuchs} and CS in Beijing to those in other locations around the world. A_{Fuchs} and CS during NPF events in this study are higher than those in Hyytiälä, similar to those observed in Boulder, and lower than those in Atlanta, Mexico City, and New Delhi. This indicates that coagulation sink in urban Beijing on NPF days is in a common range rather than higher than most other places around the world.

As shown in Eq. (1), CoagSnk is approximately proportional to the square of the particle number concentration. Nucleation intensity in urban Beijing, characterized by the number concentration of particles larger than 3 nm during typical NPF event periods, is found to be higher than in Hyytiälä and Atlanta (as shown in Fig. 6b). The number concentration of sub-3 nm particles is not accounted for to maintain comparability. Although A_{Fuchs} and CoagS represent the relative
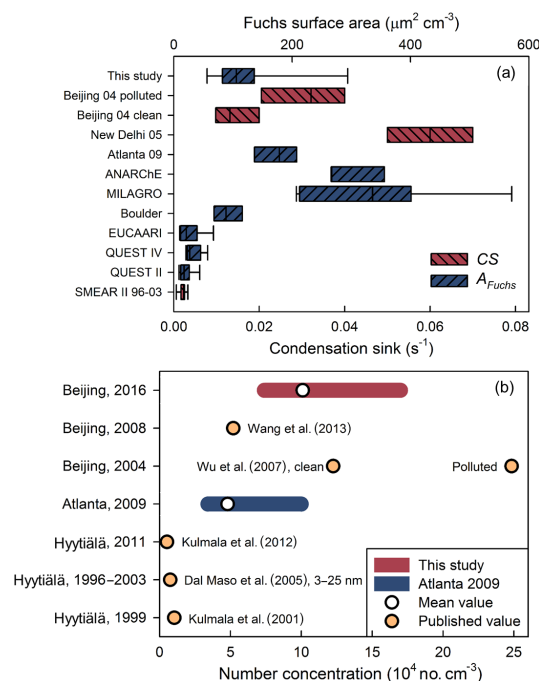

Figure 6. (a) Comparison of Fuchs surface area and condensation sink in Beijing (when NPF events occurred) with those in other locations. NPF days were classified by condensation sink in urban Beijing in 2004 (Wu et al., 2007). Condensation sink on NPF days in New Delhi was reported by Kulmala et al. (2005). ANARChE (McMurry et al., 2005) and MILAGRO (Iida et al., 2008) were conducted in Atlanta and Tecamac, respectively, while EUCCARI (Manninen et al., 2009), QUEST II (Sihto et al., 2006), and QUEST IV (Riipinen et al., 2007) were conducted at SMEAR II (Dal Maso et al., 2005) in Hyytiälä. A_{Fuchs} data in MILAGRO, ANARChE, Boulder, EUCCARI, QUEST II, and QUEST IV were published in Kuang et al. (2010). The ends of the colored rectangles correspond to quartiles, while the error bar represents the 10th and 90th percent values. **(b)** Comparison of peak number concentration of particles larger than 3 nm during NPF events in this study with those in Atlanta and other published data. Note that the published values (light orange points) in previous studies are not necessarily the mean values of the entire campaign periods.

importance of the coagulation scavenging effect (McMurry, 1983; Kulmala et al., 2001), it is the CoagSnk that reflects the number of particles lost due to coagulation scavenging in the size range of d_k to d_u. This explains the governing status of CoagSnk in estimated formation rates in urban Beijing with intense NPF events.

Figure 7 further illustrates the underestimation in new particle formation rates in China due to previously used formulae, especially for Eq. (7), which neglects coagulation among sub-25 nm particles, and Eq. (9), which simply neglects the net coagulation effect. The mean $J_{1.5}$ estimated in this study using Eq. (1) are 1.2, 2.4, and 6.4 times those estimated using Eqs. (5), (7), and (9), respectively. The mean J_3 values estimated in this study using Eq. (1) are 1.2, 2.0, and 3.3 times
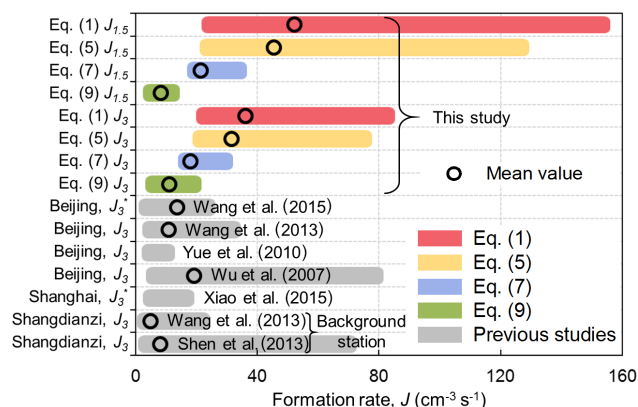
Figure 7. Estimated $J_{1.5}$ and J_3 using different equations. Previously reported J_3 values in China were included for comparison. The ends of the colored rectangles correspond to the minimum value and the maximum values, respectively. J_3^*: the upper size bound to estimate formation rate, d_u, is 6 nm (rather than 25 nm) in Wang et al. (2015) and Xiao et al. (2015).

those estimated using Eqs. (5), (7), and (9), respectively. The J_3 values reported in previous studies in urban Beijing (Wu et al., 2007; Yue et al., 2009; Wang et al., 2013, 2015), Shanghai (Xiao et al., 2015), and Shangdianzi, the regional background station of the North China Plain (Shen et al., 2011; Wang et al., 2013), are also shown in Fig. 7. Higher formation rates are anticipated if the coagulation scavenging effect is fully considered when analyzing these NPF events. Note that sub-3 nm particles are also accounted for when calculating J_3 in this study, while they are not in previous studies except for the campaign in Shanghai.

5 Conclusions

A new balance formula to estimate new particle formation rate derived from the aerosol general dynamic equation was proposed. The new formula estimates the effect of coagulation scavenging better compared to previous ones. Two criteria in determining the upper bound for calculation were proposed. An NPF campaign in urban Beijing was carried out in spring 2016. Aerosol size distributions down to ~ 1 nm were measured and used to test the new formula and those widely used in previous studies. It was found that formation rates in urban Beijing are underestimated to different extents in previously used formulae, and the underestimation of the coagulation scavenging effect (corresponding to the coagulation sink term) is the major reason. Coagulation among particles in nucleation mode was found to be important when estimating the coagulation scavenging effect in urban Beijing. The estimated formation rates of 1.5 nm particles in this campaign using the new formula were 1.3–4.3 times those estimated using the formula neglecting coagulation among particles in the nucleation mode. The coagula-

tion sink term is the governing component of the estimated formation rate in urban Beijing. Although higher than in a relatively clean atmosphere, such as in Hyytiälä, coagulation sink (expressed in the form of Fuchs surface area and condensation sink) in urban Beijing on NPF days is lower than reported in Atlanta and Mexico City. However, the number concentration of particles formed due to nucleation in urban Beijing is comparatively high, which leads to high coagulation loss. The formulae used in previous studies may perform well when describing relatively weak NPF events in a clean atmosphere, but they underestimate the coagulation scavenging effect when intense NPF events are analyzed. The formation rates reported in previous studies for urban Beijing and other locations with intense NPF events might be underestimated because of their underestimation or neglect of the coagulation scavenging effect.

Data availability. The particle size distribution data and the Matlab script for the new balance equation are available upon request.

Appendix A: Derivation of nucleation rate from aerosol general dynamic equation

The nucleation rate is the rate at which clusters grow to produce the critical cluster (nuclei). However, a more specific and microscopic definition of nucleation rate is needed for any further calculation, and it should be easily and unambiguously transferred into a mathematical expression. Here we adopt the definition based on droplet current (Eq. 10.1, Friedlander, 2000):

$$J_g = \beta_{(1,g-1)} N_1 N_{g-1} - \alpha_g s_g N_g. \tag{A1}$$

Formation rate, J_g, is the excess rate of the passage from $g-1$ (cluster or particle with $g-1$ molecules) to g by condensation over the passage from g to $g-1$ by evaporation. If g is the size of the critical cluster, J_g is defined as the nucleation rate, I. N_g is the number concentration of cluster g; $\beta_{(i,j)}$ is the coagulation coefficient of i and j, and it can be theoretically estimated from the diameter of i and j (Eq. 13.56, Seinfeld and Pandis, 2006); α_g is the monomer evaporation flux from g; and s_g is the effective surface area of g for evaporation. Only formation due to condensational growth is considered in the definition of Eq. (A1), while formation due to the coagulation of smaller clusters is not taken into account. This is based on the assumption that critical clusters are mainly formed due to the condensational growth of sulfuric acid and other chemical species. The formation of a critical cluster by coagulation does not influence the generality of the following derivation and can be readily incorporated; it will be clarified at the end of Appendix A.

The other basic equation for the derivation is the general dynamic equation in the discrete form (Eq. 11.3, Friedlander 2000):

$$\frac{dN_g}{dt} = \frac{1}{2} \sum_{\substack{i+j=g \\ i,j \geq 2}} \beta_{(i,j)} N_i N_j - \sum_{i=2}^{+\infty} \beta_{(i,g)} N_i N_g$$
$$+ \beta_{(1,g-1)} N_1 N_{g-1} - \beta_{(1,g)} N_1 N_g - \alpha_g s_g N_g$$
$$+ \alpha_{g+1} s_{g+1} N_{g+1}. \tag{A2}$$

As shown in Eq. (A2), the time rate of change of a cluster or particle number concentration, dN_g / dt on the left-hand side (LHS), is determined by formation due to the coagulation of smaller clusters and (or) particles, coagulation scavenging with preexisting clusters and particles, condensational growth from $g-1$ and to $g+1$, and evaporation to $g-1$ and from $g+1$, corresponding to the six terms on the right-hand side (RHS) of Eq. (A2). The evaporation terms (corresponding to the fifth and sixth terms on the RHS) may be zero or nearly zero when g is large; however, their exact values have no influence on derivation. An important assumption to be noted is that meteorological transport, dilution, primary emission of g, and other losses (e.g., wall loss) are not included in Eq. (A2).

Note that the last four terms on the RHS of Eq. (A2) are equal to $J_g - J_{g+1}$ by substituting Eq. (A1). By replacing the subscript g with the critical cluster size, k, we have

$$I := J_k = \frac{dN_k}{dt} + \sum_{i=2}^{+\infty} \beta_{(i,k)} N_i N_k$$
$$- \frac{1}{2} \sum_{\substack{i+j=k \\ i,j \geq 2}} \beta_{(i,j)} N_i N_j + J_{k+1}. \tag{A3}$$

The expression of Eq. (A3) is similar to Eq. (A6) in Kuang et al. (2012), which was also obtained using the balance method. J_{k+1} is usually a relatively large term in Eq. (A3), and it can be accounted for by iteration. Equation (A5) is obtained by summing Eq. (A3) from subscript k to $u-1$ as shown in Eq. (A4), where u is the particle size at the upper bound of the concerned size range.

$$I - J_{k+1} = \frac{dN_k}{dt} + \sum_{i=2}^{+\infty} \beta_{(i,k)} N_i N_k$$
$$- \frac{1}{2} \sum_{\substack{i+j=k \\ i,j \geq 2}} \beta_{(i,j)} N_i N_j$$

$$J_{k+1} - J_{k+2} = \frac{dN_{k+1}}{dt} + \sum_{i=2}^{+\infty} \beta_{(i,k+1)} N_i N_{k+1}$$
$$- \frac{1}{2} \sum_{\substack{i+j=k+1 \\ i,j \geq 2}} \beta_{(i,j)} N_i N_j \tag{A4}$$

$$\ldots = \ldots$$

$$J_{u-1} - J_u = \frac{dN_{u-1}}{dt} + \sum_{i=2}^{+\infty} \beta_{(i,u-1)} N_i N_{u-1}$$
$$- \frac{1}{2} \sum_{\substack{i+j=u-1 \\ i,j \geq 2}} \beta_{(i,j)} N_i N_j$$

$$I = \frac{d \sum_{g=k}^{u-1} N_g}{dt} + \sum_{g=k}^{u-1} \sum_{i=2}^{+\infty} \beta_{(i,g)} N_i N_g$$
$$- \frac{1}{2} \sum_{g=k}^{u-1} \sum_{\substack{i+j=g \\ i,j \geq 2}} \beta_{(i,j)} N_i N_j + J_u \tag{A5}$$

On the RHS of Eq. (A5) are the time rate of change of the particle concentration, the coagulation sink term, the coagulation source term, and the condensational growth term. Note that when particle u is large enough, J_u is nearly zero, i.e., $\lim_{u \to \infty} J_u = 0$ because of the negligible condensational growth

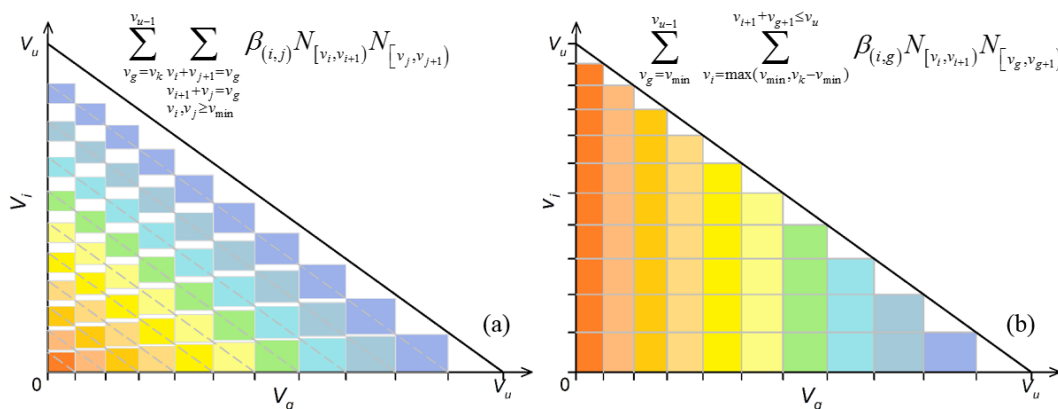**Figure A1.** Schematic for two different summation sequences to estimate the coagulation source term. Equations in panels **(a)** and **(b)** correspond to the continuous forms on the far LHS and the far RHS formulae in Eq. (A7), respectively. The coagulation source term is denoted by half the area of the triangle (since the particles at the same diameter are accounted for twice). The colored areas are the estimated area using the two equations. The summation terms corresponding to the same particle volume, v_g, are shown in the same color. The coagulation source term is underestimated in panel **(a)** because v_g increases nonlinearly in this case, whereas the estimated coagulation source term is independent of the bin structures for d_g and d_i in panel **(b)**.

and low number concentration compared to those of freshly nucleated small particles. Equation (A6) is obtained by replacing the upper bound, u, with infinity and further simplified by combining the second and third term on the RHS of Eq. (A5).

$$I = \frac{\mathrm{d}\sum_{g=k}^{+\infty} N_g}{\partial t} + \frac{1}{2}\sum_{g=k}^{+\infty}\sum_{i=k}^{+\infty}\beta_{(i,g)}N_i N_g \qquad (A6)$$

Theoretically, Eq. (A6) can be used to estimate I since each term on the RHS can be calculated. However, the validity of Eq. (A6) faces a higher risk of violation when applied in a real atmosphere due to non-negligible primary emission sources. This is because Eq. (A6) is a balance equation for the whole aerosol population rather than a limited size range of the nucleation mode. It is both more cautious and efficient to use Eq. (A5) with a proper particle size u and a reasonable estimation of J_u.

When using measured particle size distribution to estimate I, Eq. (A5) has to be converted from the discrete form into the continuous form. For the third term on the RHS of Eq. (A5), i.e., the coagulation source term, its summation sequence can be rearranged as

$$\frac{1}{2}\sum_{g=k}^{u-1}\sum_{\substack{i+j=g \\ i,j\geq 2}}\beta_{(i,j)}N_i N_j$$

$$= \frac{1}{2}\beta_{(2,k-2)}N_2 N_{k-2} + \ldots + \frac{1}{2}\beta_{(k-2,2)}N_{k-2}N_2$$

$$+ \ldots$$

$$+ \frac{1}{2}\beta_{(2,u-3)}N_2 N_{u-3} + \ldots + \frac{1}{2}\beta_{(k-2,u-k+1)}N_{k-2}N_{u-k+1}$$

$$+ \ldots + \frac{1}{2}\beta_{(u-3,2)}N_{u-3}N_2$$

$$= \frac{1}{2}\sum_{g=2}^{u-3}\sum_{i=\max(2,k-g)}^{i+g\leq u-1}\beta_{(i,g)}N_i N_g. \qquad (A7)$$

The formulae on both the far LHS and the far RHS of Eq. (A7) are equally accurate to estimate the coagulation source term. However, simply substituting the continuous particle diameter (e.g., d_g) for the discrete size (e.g., g) on the far LHS of Eq. (A7) will result in uncertainties when the size bins do not increase linearly in the particle volume space. As indicated in Fig. A1, substituting the continuous particle diameter for the discrete size on the far RHS of Eq. (A7) is independent of the bin structure for d_g and d_i.

Thus, Eq. (A5) can be rewritten as

$$I = \frac{\mathrm{d}N_{[d_k,d_u]}}{\mathrm{d}t} + \sum_{d_g=d_k}^{d_{u-1}}\sum_{d_i=d_{\min}}^{+\infty}\beta_{(i,g)}N_{[d_i,d_{i+1}]}N_{[d_g,d_{g+1}]}$$

$$- \frac{1}{2}\sum_{d_g=d_{\min}}^{d_{u-1}}\sum_{d_i^3=\max(d_{\min}^3,d_k^3-d_{\min}^3)}^{d_{i+1}^3+d_{g+1}^3\leq d_u^3}\beta_{(i,g)}N_{[d_i,d_{i+1}]}$$

$$N_{[d_g,d_{g+1}]} + J_u, \qquad (A8)$$

where $d_{\min}$ is theoretically the minimum cluster size. Note that the size bin from d_{u-1} to d_u is denoted by the subscript $u-1$, so the upper bound of the size range for calculation is d_u. The discrete upper sizes, $u-1$ in Eq. (A5) and $u-3$ in Eq. (A7), are approximated by d_u in Eq. (A8). $N_{[d_k,d_u]}$ is defined as the number concentration in the size range from d_k to d_u (particles with diameters of d_u are not accounted for), corresponding to $\sum_{g=k}^{u-1} N_g$ in the discrete from. Since measured

size bins are finite, Eq. (A8) is expressed in the summation form rather than the integration form. Practically, Eq. (A8) is only an estimation of Eq. (A5) because coagulation is calculated by using size bins, while the particles sizes in each size bin are not exactly the same as the representing diameter, d_g. The upper size bound, d_u, is a "properly large" size at which diameter J_u is negligible compared to the sum of the other three terms on the RHS of Eq. (A8). Properly large is defined by the following two criteria: d_u should not be too large so that the calculated nucleation rate is non-negligibly affected by transport or primary emissions, and d_u should not be too small so that the calculated nucleation rate is underestimated because J_u is still too large to be neglected or to be estimated by growth rate (as illustrated in the following paragraph). These two criteria seem to be contradictory; however, as illustrated in Fig. 2b, the calculated nucleation rate is usually not sensitive to the upper bound because J_u decreases rapidly with the increase in d_u since the freshly nucleated particles are usually in a relatively narrow size range, especially during strong NPF events.

The fourth term on the RHS of Eq. (A8), J_u, is usually so small that it can be simply neglected when d_u is properly large. However, an approximate term is recommended for better estimation. Here we introduce a sufficient but possibly unnecessary condition that the net coagulation effect between any particle larger than d_u and other particles can be neglected when estimating the GR term. Define $N_{[d_u,d_u+\Delta d)}\big|_t$ as the number concentration of particles in a narrow size range from d_u to $d_u + \Delta d$ at time t. After a very short time dt, these particles grow into the size range from $d_u + dd$ to $d_u + \Delta d + dd$, which is based on the assumption that diameter growth is equal for different particles in such a narrow size and time range, while the number concentration remains the same since there is no particle loss. Particles in the size range from $d_u + \Delta d$ to $+\infty$ at time t grow to the size range from $d_u + \Delta d + dd$ to $+\infty$. Since the size range is narrow enough, it is reasonable to assume that the concentration of particles is equally distributed in the size range from d_u to $d_u + \Delta d + dd$, i.e.,

$$\frac{N_{[d_i,d_j)}\big|_{t+dt}}{N_{[d_m,d_n)}\big|_{t+dt}} = \frac{d_j - d_i}{d_n - d_m},$$
$$\text{for any } d_i, d_j, d_m, d_n \in [d_u, d_u + \Delta d + dd). \quad (A9)$$

The particle size distribution function, n, and growth rate, GR, are defined as Eqs. (A10) and (A11), respectively. Equation (A12) is obtained by combining Eqs. (A6), (A9), (A10), and (A11).

$$n_u = \frac{dN}{dd}\bigg|_{d_u} = \lim_{\Delta d \to 0} \frac{N_{[d_u,d_u+\Delta d)}}{\Delta d} \quad (A10)$$

$$GR_u = \frac{dd}{dt}\bigg|_{d_u} \quad (A11)$$

$$J_u = \frac{dN_{[d_u,+\infty)}}{dt}$$
$$= \frac{N_{[d_u,d_u+dd)}\big|_{t+dt} + N_{[d_u+dd,+\infty)}\big|_{t+dt} - N_{[d_u,+\infty)}\big|_t}{dt}$$
$$= \frac{N_{[d_u,d_u+dd)}\big|_{t+dt}}{dt}$$
$$= \lim_{\Delta d \to 0} \frac{N_{[d_u,d_u+dd)}\big|_{t+dt}}{N_{[d_u+dd,d_u+\Delta d+dd)}\big|_{t+dt} \cdot dt}$$
$$\cdot N_{[d_u+dd,d_u+\Delta d+dd)}\big|_{t+dt}$$
$$= \lim_{\Delta d \to 0} \frac{dd}{\Delta d \cdot dt} \cdot N_{[d_u,d_u+\Delta d)}\big|_t$$
$$= n_u \cdot GR_u \quad (A12)$$

Finally by combining Eqs. (A8) and (A12), we can obtain the equation to estimate the nucleation rate as Eq. (A13):

$$I = \frac{dN_{[d_k,d_u)}}{dt} + \sum_{d_g=d_k}^{d_{u-1}} \sum_{d_i=d_{\min}}^{+\infty} \beta_{(i,g)} N_{[d_i,d_{i+1})} N_{[d_g,d_{g+1})}$$
$$- \frac{1}{2} \sum_{d_g=d_{\min}}^{d_{u-1}} \sum_{d_i^3=\max(d_{\min}^3,d_k^3-d_{\min}^3)}^{d_{i+1}^3+d_{g+1}^3 \le d_u^3} \beta_{(i,g)} N_{[d_i,d_{i+1})} N_{[d_g,d_{g+1})} + n_u \cdot GR_u. \quad (A13)$$

The first term on the RHS of Eq. (A13) is the change in the number concentration of particles ranged from d_k to d_u. The second and third terms are particle loss to coagulation scavenging and particle formation by coagulation, named as the coagulation sink term (CoagSnk) and the coagulation source term (CoagSrc), respectively (Kuang et al, 2012). The fourth term is the condensational growth term, which is an approximation of the formation rate, J_u. This balance formula derived from the aerosol general dynamic equation can also be expressed as Eq. (A14):

$$I = \frac{dN_{[d_k,d_u)}}{dt} + \text{CoagSnk} - \text{CoagSrc} + n_u \cdot GR_u. \quad (A14)$$

When applying Eq. (A13) in practice, d_k is usually the assumed size of the critical nuclei (or the lowest size limit of the instrument, corresponding to the formation rate, J_k, rather than the nucleation rate, I). The dN / dt term can be obtained either by differentiating between adjacent time bins or fitting in a continuous time period. CoagSnk and CoagSrc can be directly calculated from the particle size distribution, where $d_{\min}$ is the minimum detected particle diameter. If formation by the coagulation of smaller clusters is also included in the definition of nucleation rate, the calculation of CoagSrc (the third term on the RHS of Eq. A12) should begin with d_{k+1} instead of d_k, which usually has little effect since the difference is only a size bin and CoagSrc is usually a minor term of J in the atmospheric environment. The growth rate can be estimated by using different methods (Weber et al., 1996, 1997; Kulmala et al., 2012; Lehtipalo et al., 2014), or

the growth term can simply be neglected when d_u is properly large.

It should be clarified that the formation rate calculated using Eq. (A13) may be underestimated because coagulation scavenging by particles and clusters smaller than d_{min} is neglected due to the limitation of measuring instruments. As illustrated in Fig. 6a, CoagSnk calculated using d_p larger than 3 nm is $\sim 89.1\%$ of that using d_p larger than 1.5 nm. It could be inferred that the calculated J_3 was slightly underestimated in previous studies lacking size distributions for sub-3 nm particles. In this study, measured particles down to 1.3 nm are accounted for when calculating $J_{1.5}$ and J_3. Neglecting coagulation between clusters may also have a non-negligible effect on the calculated results (McMurry, 1983), which calls for the measurement of major molecular clusters participating in nucleation if a more accurate formation rate is to be obtained.

Appendix B: Relationships with previous approaches

Since the new balance approach proposed in this study is based on the aerosol general dynamic equation with a reasonable assumption that the net coagulation of any particle larger than the properly large upper bound, d_u, and other particles can be neglected, its inter-relationships with former approaches can be elucidated by making additional assumptions and approximations.

The formation rate is defined as the flux growth of particles past a given size and can be expressed as Eq. (B1), where k is the number of molecules contained by the particle (Heisler and Friedlander, 1977; Weber et al., 1996; Kuang et al., 2008, 2012). Note that Eq. (B1) is valid only when it is in the continuous space of particle diameter, while a more accurate expression in the discrete form is shown as Eq. (B2).

$$J_k = n_k \cdot GR_k \tag{B1}$$
$$J_k = n_{k-1} \cdot GR_{k-1} \tag{B2}$$

Equation (B2) is believed to be theoretically correct since the only condensational flux into d_k is the growth of smaller clusters or particles with diameter d_{k-1}. Although similar in expression to Eq. (A12), Eq. (B2) focuses on the flux into rather than out of the size bin for calculation, and there is no need to account for coagulation scavenging, as illustrated in Fig. 1.

A theoretical expression of GR proposed in a previous study is shown as Eq. (B3), where α is herein the coagulation efficiency (fraction of collisions that successfully result in coagulation), V_1 is the volume increment when adding a single gaseous precursor, and v is the mean thermal velocity of the gaseous precursor (Weber et al., 1996). Here we update the equation by considering different chemical species and describing coagulation by β, as shown in Eq. (B4). The subscript c denotes different chemical species of monomers participating in the condensational growth of cluster $k-1$,
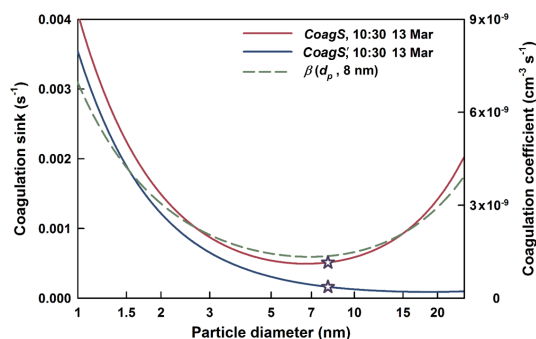

Figure B1. Coagulation coefficient and calculated coagulation sink during a typical NPF event. CoagS and CoagS′ are defined in Eqs. (B7) and (B8), respectively, and d_m in this figure is treated as a variable rather than a constant value. The upper and lower stars denote $CoagS'_{8\,nm}$ and $CoagS_{8\,nm}$, which are used in the second term on the RHS of Eqs. (5) and (6), respectively, to approximate CoagSnk.
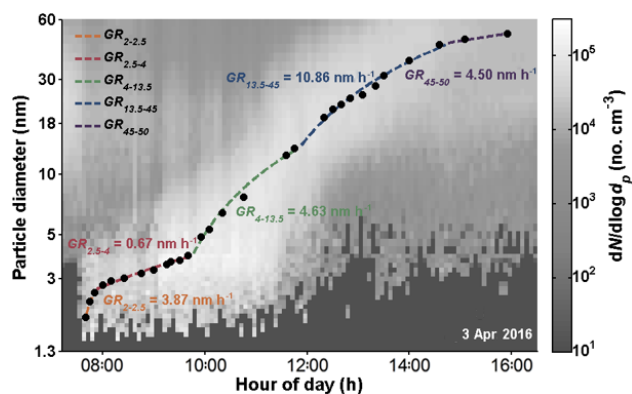

Figure B2. Size- and time-dependent growth rate on an NPF day observed in Beijing. Representative diameters are obtained by log-normal fitting of nucleation mode particles in each time bin, and GR is linearly fitted in each section.

and N_{1c} is their corresponding number concentration. Coagulation efficiency is included in each $\beta_{(1c,k)}$ (Eq. 13.56, Seinfeld and Pandis, 2006).

$$GR_k = \frac{\alpha V_1 N_1 v}{2} \tag{B3}$$

$$GR_{k-1} = \frac{\sum_c \beta_{(1c,k-1)} N_{1c} N_{k-1}}{n_{k-1}} \tag{B4}$$

Equation (B2) is theoretically correct; however, it faces difficulties when being applied in practice since n_{k-1} is obtained by approximation over a size range around d_k rather than the true frequency density at cluster $k-1$, dN_{k-1}/dd_{k-1}. Moreover, because a size distribution smaller than d_k is difficult to obtain, the size range for estimation is usually larger than d_k. For example, the formula to estimate J_3 using nano-SMPS data in Kuang et al. (2008) is shown as Eq. (B5). Although

Eq. (B5) seems to be an estimation of Eq. (B2), they are essentially two different equations. This is because the measured particle number concentration in the size range for calculation, i.e., N_{3-6} in Eq. (B5), has been affected by coagulation. By comparing with Eq. (A14), it can be concluded that dN / dt, CoagSnk, and CoagSrc are simply neglected in Eq. (B5), while Eq. (B2) is not subject to this problem by its definition.

$$J_3 \approx \frac{N_{3-6}}{3\,\text{nm}} \cdot \text{GR}_{1-3} \tag{B5}$$

There are also problems in estimating GR_{k-1}. Equation (B4) is only a theoretical formula since it is nearly impossible to determine all the chemical species contributing to nucleation and their corresponding coagulation coefficients in the complicated atmospheric environment. GR calculated from sulfuric acid using Eq. (B3) may lead to underestimation (Kuang et al., 2010), while uncertainties also exist in the approaches that fit particle size distributions to obtain GR (Kulmala et al., 2012; Lehtipalo et al., 2014) because the effect of coagulation on measured size distribution is also neglected. So conclusively, Eq. (B2) is considered to be theoretically correct; however, it is not recommend to be applied for analyzing NPF events with high coagulation scavenging.

The other approach is a balance method based on a macroscopic point of view shown as Eq. (B6) (Kulmala et al., 2001, 2004), and we adopt the equation in the most recent paper (Kulmala et al., 2012). Usually d_m is the geometric mean diameter of d_k and d_u. However, coagulation between any particle smaller than d_m or even d_u and another particle (with any size) is sometimes neglected when it comes to calculation, such as the formula suggested in Kulmala et al. (2012) shown as Eq. (B7).

$$J_k = \frac{dN_{[d_k,d_u]}}{dt} + \text{CoagS}_m \cdot N_{[d_k,d_u]} + \frac{N_{[d_k,d_u]}}{(d_u - d_k)} \cdot \text{GR}_{[d_k,d_u]} \tag{B6}$$

$$\text{CoagS}'_m = \sum_{d_i=d_m}^{+\infty} \beta_{(i,m)} N_i \tag{B7}$$

Equation (B6) appears similar to Eq. (A14) since they both originate from the population balance method; however, there are some differences between them.

First, the upper bound for particle size in Eq. (B6), d_u, lacks a strict definition and discussion. As discussed in Appendix A, d_u should be decided by the two criteria that the effects of transport and primary emissions are negligible and the condensational growth term, J_u, is relatively small compared to J_k. The upper bound of 25 nm is usually reasonable since a high concentration of particles formed by nucleation predominates the coagulation sink term during strong new particle formation times, while the upper bound of 6 nm may lead to underestimation when freshly formed particles grow larger, as discussed in the main text.

Second, scavenging by coagulation with particles smaller than d_m is not included if using Eq. (B7) to calculate CoagS.

As shown in Fig. B1, CoagS is always larger than CoagS′, and their difference increases as d_m increases. $\text{CoagS}'_{8\,\text{nm}}$ is $\sim 31\%$ of $\text{CoagS}_{8\,\text{nm}}$, indicating a large amount of underestimation when using Eq. (B7). Note that Eq. (3) and the approximation formula (estimated with condensation sink) proposed by Lehtinen et al. (2007) do not suffer from this problem.

Third, the second term on the RHS of Eq. (B6) is not always a reasonable approximation of CoagSnk in Eqs. (A13) and (A14). Theoretically, the relationship between CoagSnk and CoagS is shown as Eq. (B8), while CoagS_m is chosen as the representative value when estimating J using Eq. (B6).

$$\text{CoagSnk} = \sum_{d_g=d_k}^{d_u} \text{CoagS}_g \cdot N_g \tag{B8}$$

However, CoagS is not a relatively constant value versus particle diameter, and CoagS_m is not the mean value of CoagS in the calculated size range from d_k to d_u. As illustrated in Fig. B1, the coagulation coefficient with 8 nm particles decreases rapidly with the increase in d_i when particle is smaller than 8 nm. The minimum value of $\beta_{(d_i,8\,\text{nm})}$ appears at d_i around 8 nm because particles with similar thermal velocities are more difficult to collide with each other. The calculated CoagS′ during a strong NPF event on 27 March 2016 appears to monotonously decrease with the increase in d_m, while the calculated CoagS has a minimum value of 6.7 nm because CoagS is mainly attributed to nucleation mode particles during NPF events. In this example, $\text{CoagS}_{8\,\text{nm}}$ and $\text{CoagS}'_{8\,\text{nm}}$ are ~ 22.6 and $\sim 7.2\%$ of $\text{CoagS}_{1.5\,\text{nm}}$, respectively, indicating a non-negligible underestimation of the coagulation sink term and nucleation rate when using a constant CoagS_m instead of a varying value (as a function of particle diameter).

Fourth, particle formation by coagulation is neglected in Eq. (B6). The absence of CoagSrc will lead to an overestimation of the nucleation rate. However, it sometimes coincidently cancels out the underestimation caused by using CoagS_m to approximate CoagSrc, as discussed in the main text.

Fifth, the growth term in Eq. (B6) is estimated over the whole size range from d_k to d_u, while in Eq. (A13) it is mathematically restricted at the upper bound, d_u; n_u is usually smaller than the mean value in the size range from d_k to d_u during an NPF event, and recent work has revealed that the observed GR is size dependent (Kuang et al., 2012; Kulmala et al., 2013; Xiao et al., 2015). For example, as shown in Fig. B2, GR varies with time in the NPF event on 3 April 2016 and was linearly fitted in different diameter ranges. The mean GR of particles in the size range from 2 to 25 nm is $\sim 7.47\,\text{nm}\,\text{h}^{-1}$, while GR_{25} is $\sim 10.86\,\text{nm}\,\text{h}^{-1}$. At 11:30 on 3 April, n_{25} ($dN / d\log d_p$ at 25 nm) is 164 no. cm^{-3}, while the mean n of particles in the size range from 2 to 25 nm is 4755 no. cm^{-3}. The calculated

condensational growth term in Eq. (B6) is ~ 20 times of that in Eq. (A13).

In a relatively clean environment with weak NPF events, Eq. (B6) may work well since the calculated J_k is mainly predominated by $\mathrm{d}N / \mathrm{d}t$. However, when the number concentration of aerosol formed by nucleation and (or) background aerosol is high, i.e., when CoagSnk is the major component of J_k, Eq. (B6) underestimates the formation rate (and nucleation rate) due to underestimation of the coagulation scavenging effect.

References

Aitken, J.: On some nuclei of cloudy condensation, P. Roy. Soc. Edinb., XXXI, 495–511, 1911.

An, J., Wang, H., Shen, L., Zhu, B., Zou, J., Gao, J., and Kang, H.: Characteristics of new particle formation events in Nanjing, China: Effect of water-soluble ions, Atmos. Environ., 108, 32–40, https://doi.org/10.1016/j.atmosenv.2015.01.038, 2015.

Cai, R., Chen, D.-R., Hao, J., and Jiang, J.: A miniature cylindrical differential mobility analyzer for sub-3 nm particle sizing, J. Aerosol Sci., 106, 111–119, https://doi.org/10.1016/j.jaerosci.2017.01.004, 2017.

Cao, C., Jiang, W., Wang, B., Fang, J., Lang, J., Tian, G., Jiang, J., and Zhu, T. F.: Inhalable microorganisms in Beijing's $PM_{2.5}$ and PM_{10} pollutants during a severe smog event, Environ. Sci. Technol., 48, 1499–1507, https://doi.org/10.1021/es4048472, 2014.

Clarke, A. D., Davis, D., Kapustin, V. N., Eisele, F., Chen, G., Paluch, I., Lenschow, D., Bandy, A. R., Thornton, D., Moore, K., Mauldin, L., Tanner, D., Litchy, M., Carroll, M. A., Collins, J., and Albercook, G.: Particle nucleation in the tropical boundary layer and its coupling to marine sulfur sources, Science, 282, 89–92, https://doi.org/10.1126/science.282.5386.89, 1998.

Covert, D. S., Kapustin, V. N., Quinn, P. K., and Bates, T. S.: New particle formation in the marine boundary layer, J. Geophys. Res., 97, 20518–20589, 1992.

Covert, D. S., Wiedensohler, A., Aalto, P., Heintzenberg, J., McMurry, P. H., and Leck, C.: Aerosol number size distributions from 3 to 500 nm diameter in the arctic marine boundary layer during summer and autumn, Tellus B, 48, 197–212, https://doi.org/10.1034/j.1600-0889.1996.t01-1-00005.x, 1996.

Dal Maso, M., Kulmala, M., Riipinen, I., Wagner, R., Hussein, T., Aalto, P., and Lehtinen, K. E.: Formation and growth of fresh atmospheric aerosols: eight years of aerosol size distribution data from SMEAR II, Hyytiälä, Finland, Boreal Environ. Res., 10, 323–336, 2005.

Franchin, A., Downard, A., Kangasluoma, J., Nieminen, T., Lehtipalo, K., Steiner, G., Manninen, H. E., Petäjä, T., Flagan, R. C., and Kulmala, M.: A new high-transmission inlet for the Caltech nano-RDMA for size distribution measurements of sub-3 nm ions at ambient concentrations, Atmos. Meas. Tech., 9, 2709–2720, https://doi.org/10.5194/amt-9-2709-2016, 2016.

Friedlander, S. K.: Smoke, dust and haze, 2nd Edn., Topics in Chemical Engineering, edited by: Gubbins, K. E., Oxford University Press, New York, 2000.

Hagen, D. E. and Alofs, D. J.: Linear Inversion Method to Obtain aerosol Size Distributions from Measurements with a Differential Mobility Analyzer, Aerosol Sci. Tech., 2, 465–475, 1983.

He, K., Yang, F., Ma, Y., Zhang, Q., Yao, X., Chan, C. K., Cadel, S., Chan, T., and Mulawa, P.: The characteristics of $PM_{2.5}$ in Beijing, China, Atmos. Environ., 35, 4959–4970, 2001.

Heisler, S. L. and Friedlander, S. K.: Gas-to-particle conversion in photochemical smog: Aerosol growth laws and mechanisms for organics, Atmos. Environ., 11, 157–168, https://doi.org/10.1016/0004-6981(77)90220-7, 1977.

Hu, M., Peng, J., Sun, K., Yue, D., Guo, S., Wiedensohler, A., and Wu, Z.: Estimation of size-resolved ambient particle density based on the measurement of aerosol number, mass, and chemical size distributions in the winter in Beijing, Environ. Sci. Technol., 46, 9941–9947, https://doi.org/10.1021/es204073t, 2012.

Iida, K., Stolzenburg, M., McMurry, P., Dunn, M. J., Smith, J. N., Eisele, F., and Keady, P.: Contribution of ion-induced nucleation to new particle formation: Methodology and its application to atmospheric observations in Boulder, Colorado, J. Geophys. Res.-Atmos., 111, D23201, https://doi.org/10.1029/2006jd007167, 2006.

Iida, K., Stolzenburg, M. R., McMurry, P. H., and Smith, J. N.: Estimating nanoparticle growth rates from size-dependent charged fractions: Analysis of new particle formation events in Mexico City, J. Geophys. Res.-Atmos., 113, D05207, https://doi.org/10.1029/2007jd009260, 2008.

Iida, K., Stolzenburg, M. R., and McMurry, P. H.: Effect of Working Fluid on Sub-2 nm Particle Detection with a Laminar Flow Ultrafine Condensation Particle Counter, Aerosol Sci. Tech., 43, 81–96, https://doi.org/10.1080/02786820802488194, 2009.

Jiang, J., Chen, M., Kuang, C., Attoui, M., and McMurry, P. H.: Electrical Mobility Spectrometer Using a Diethylene Glycol Condensation Particle Counter for Measurement of Aerosol Size Distributions Down to 1 nm, Aerosol Sci. Tech., 45, 510–521, https://doi.org/10.1080/02786826.2010.547538, 2011a.

Jiang, J., Zhao, J., Chen, M., Eisele, F. L., Scheckman, J., Williams, B. J., Kuang, C., and McMurry, P. H.: First Measurements of Neutral Atmospheric Cluster and 1–2 nm Particle Number Size Distributions During Nucleation Events, Aerosol Sci. Tech., 45, , ii–v, https://doi.org/10.1080/02786826.2010.546817, 2011b.

Kerminen, V.-M., Paramonov, M., Anttila, T., Riipinen, I., Fountoukis, C., Korhonen, H., Asmi, E., Laakso, L., Lihavainen, H., Swietlicki, E., Svenningsson, B., Asmi, A., Pandis, S. N., Kulmala, M., and Petäjä, T.: Cloud condensation nuclei production associated with atmospheric nucleation: a synthesis based on existing literature and new results, Atmos. Chem. Phys., 12, 12037–12059, https://doi.org/10.5194/acp-12-12037-2012, 2012.

Kuang, C., McMurry, P. H., McCormick, A. V., and Eisele, F. L.: Dependence of nucleation rates on sulfuric acid vapor concentration in diverse atmospheric locations, J. Geophys. Res., 113, D10209, https://doi.org/10.1029/2007jd009253, 2008.

Kuang, C., McMurry, P. H., and McCormick, A. V.: Determination of cloud condensation nuclei production from measured new particle formation events, Geophys. Res. Lett., 36, L09822, https://doi.org/10.1029/2009gl037584, 2009.

Kuang, C., Riipinen, I., Sihto, S.-L., Kulmala, M., McCormick, A. V., and McMurry, P. H.: An improved criterion for new particle formation in diverse atmospheric environments, Atmos.

Chem. Phys., 10, 8469–8480, https://doi.org/10.5194/acp-10-8469-2010, 2010.

Kuang, C., Chen, M., Zhao, J., Smith, J., McMurry, P. H., and Wang, J.: Size and time-resolved growth rate measurements of 1 to 5 nm freshly formed atmospheric nuclei, Atmos. Chem. Phys., 12, 3573–3589, https://doi.org/10.5194/acp-12-3573-2012, 2012.

Kulmala, M., Dal Maso, M., Mäkelä, J. M., Pirjola, L., Väkevä, M., Aalto, P., Miikkulainen, P., Hämeri, K., and O'dowd, C. D.: On the formation, growth and composition of nucleation mode particles, Tellus, 53, 479–490, 2001.

Kulmala, M., Vehkamäki, H., Petäjä, T., Dal Maso, M., Lauri, A., Kerminen, V. M., Birmili, W., and McMurry, P. H.: Formation and growth rates of ultrafine atmospheric particles: a review of observations, J. Aerosol Sci., 35, 143–176, https://doi.org/10.1016/j.jaerosci.2003.10.003, 2004.

Kulmala, M., Petäjä, T., Mönkkönen, P., Koponen, I. K., Dal Maso, M., Aalto, P. P., Lehtinen, K. E. J., and Kerminen, V.-M.: On the growth of nucleation mode particles: source rates of condensable vapor in polluted and clean environments, Atmos. Chem. Phys., 5, 409–416, https://doi.org/10.5194/acp-5-409-2005, 2005.

Kulmala, M., Petäjä, T., Nieminen, T., Sipilä, M., Manninen, H. E., Lehtipalo, K., Dal Maso, M., Aalto, P. P., Junninen, H., Paasonen, P., Riipinen, I., Lehtinen, K. E., Laaksonen, A., and Kerminen, V. M.: Measurement of the nucleation of atmospheric aerosol particles, Nat. Protoc., 7, 1651–1667, https://doi.org/10.1038/nprot.2012.091, 2012.

Kulmala, M., Kontkanen, J., Junninen, H., Lehtipalo, K., Manninen, H. E., Nieminen, T., Petäjä, T., Sipilä, M., Schobesberger, S., Rantala, P., Franchin, A., Jokinen, T., Jarvinen, E., Äijälä, M., Kangasluoma, J., Hakala, J., Aalto, P. P., Paasonen, P., Mikkilä, J., Vanhanen, J., Aalto, J., Hakola, H., Makkonen, U., Ruuskanen, T., Mauldin III, R. L., Duplissy, J., Vehkamäki, H., Bäck, J., Kortelainen, A., Riipinen, I., Kurtén, T., Johnston, M. V., Smith, J. N., Ehn, M., Mentel, T. F., Lehtinen, K. E., Laaksonen, A., Kerminen, V.-M., and Worsnop, D. R.: Direct observations of atmospheric aerosol nucleation, Science, 339, 943–946, https://doi.org/10.1126/science.1227385, 2013.

Kulmala, M., Petäjä, T., Kerminen, V. M., Kujansuu, J., Ruuskanen, T., Ding, A. J., Nie, W., Hu, M., Wang, Z., Wu, Z., Wang, L., and Worsnop, D. R.: On secondary new particle formation in China, Frontiers of Environ. Sci. Eng., 10, 191–200, https://doi.org/10.1007/s11783-016-0850-1, 2016.

Lee, S.-H., Reeves, J. M., Wilson, J. C., Hunton, D. E., Viggiano, A. A., Miller, T. M., Ballenthin, J. O., and Lait, L. R.: Particle formation by ion nucleation in the upper troposphere and lower stratosphere, Science, 301, 1886–1889, https://doi.org/10.1126/science.1087236, 2003.

Lehtinen, K. E. J., Dal Maso, M., Kulmala, M., and Kerminen, V.-M.: Estimating nucleation rates from apparent particle formation rates and vice versa: Revised formulation of the Kerminen–Kulmala equation, J. Aerosol Sci., 38, 988–994, https://doi.org/10.1016/j.jaerosci.2007.06.009, 2007.

Lehtipalo, K., Leppä, J., Kontkanen, J., Kangasluoma, J., Franchin, A., Wimmer, D., Schobesberger, S., Junninen, H., Petäjä, T., Sipilä, M., Mikkilä, J., Vanhanen, J., Worsnop, D. R., and Kulmala, M.: Methods for determining particle size distribution and growth rates between 1 and 3 nm using the Particle Size Magnifier, Boreal Environ. Res., 19, 215–236, 2014.

Leng, C., Zhang, Q., Tao, J., Zhang, H., Zhang, D., Xu, C., Li, X., Kong, L., Cheng, T., Zhang, R., Yang, X., Chen, J., Qiao, L., Lou, S., Wang, H., and Chen, C.: Impacts of new particle formation on aerosol cloud condensation nuclei (CCN) activity in Shanghai: case study, Atmos. Chem. Phys., 14, 11353–11365, https://doi.org/10.5194/acp-14-11353-2014, 2014.

Liu, J., Jiang, J., Zhang, Q., Deng, J., and Hao, J.: A spectrometer for measuring particle size distributions in the range of 3 nm to 10 μm, Frontiers of Environmental Science & Engineering, 10, 63–72, https://doi.org/10.1007/s11783-014-0754-x, 2016.

Lohmann, U. and Feichter, J.: Global indirect aerosol effects: a review, Atmospheric Chemistry and Physics, 5, 715–737, https://doi.org/10.5194/acp-5-715-2005, 2005.

Manninen, H. E., Nieminen, T., Riipinen, I., Yli-Juuti, T., Gagné, S., Asmi, E., Aalto, P. P., Petäjä, T., Kerminen, V.-M., and Kulmala, M.: Charged and total particle formation and growth rates during EUCAARI 2007 campaign in Hyytiälä, Atmos. Chem. Phys., 9, 4077–4089, https://doi.org/10.5194/acp-9-4077-2009, 2009.

McMurry, P. H.: New particle formation in the presence of an aerosol: rates, time scales, and sub-0.01 μm size distributions, J. Colloid Interf. Sci., 95, 72–80, 1983.

McMurry, P. H., Fink, M., Sakurai, H., Stolzenburg, M. R., Mauldin, R. L., Smith, J., Eisele, F., Moore, K., Sjostedt, S., Tanner, D., Huey, L. G., Nowak, J. B., Edgerton, E., and Voisin, D.: A criterion for new particle formation in the sulfur-rich Atlanta atmosphere, J. Geophys. Res., 110, D22S02, https://doi.org/10.1029/2005jd005901, 2005.

Misaki, M.: Mobility spectrums of large Ions in the new Mexico semidesert, J. Geophys. Res., 69, 3309–3318, 1964.

Paasonen, P., Sihto, S.-L., Nieminen, T., Vuollekoski, H., Riipinen, I., Plaß-Dülmer, C., Berresheim, H., Birmili, W., and Kulmala, M.: Connection between new particle formation and sulphuric acid at Hohenpeissenberg (Germany) including the influence of organic compounds, Boreal Environ. Res., 14, 616–629, 2009.

Park, J., Sakurai, H., Vollmers, K., and McMurry, P. H.: Aerosol size distributions measured at the South Pole during ISCAT, Atmos. Environ., 38, 5493–5500, https://doi.org/10.1016/j.atmosenv.2002.12.001, 2004.

Qi, X. M., Ding, A. J., Nie, W., Petäjä, T., Kerminen, V.-M., Herrmann, E., Xie, Y. N., Zheng, L. F., Manninen, H., Aalto, P., Sun, J. N., Xu, Z. N., Chi, X. G., Huang, X., Boy, M., Virkkula, A., Yang, X.-Q., Fu, C. B., and Kulmala, M.: Aerosol size distribution and new particle formation in the western Yangtze River Delta of China: 2 years of measurements at the SORPES station, Atmos. Chem. Phys., 15, 12445–12464, https://doi.org/10.5194/acp-15-12445-2015, 2015.

Riipinen, I., Sihto, S.-L., Kulmala, M., Arnold, F., Dal Maso, M., Birmili, W., Saarnio, K., Teinilä, K., Kerminen, V.-M., Laaksonen, A., and Lehtinen, K. E. J.: Connections between atmospheric sulphuric acid and new particle formation during QUEST III-IV campaigns in Heidelberg and Hyytiälä, Atmos. Chem. Phys., 7, 1899–1914, https://doi.org/10.5194/acp-7-1899-2007, 2007.

Seinfeld, J. H. and Pandis, S. N.: Atmospheric Chemistry and Physics, 2nd Edn., John Wiley & Sons, Inc., New Jersey, 2006.

Shen, X. J., Sun, J. Y., Zhang, Y. M., Wehner, B., Nowak, A., Tuch, T., Zhang, X. C., Wang, T. T., Zhou, H. G., Zhang, X. L., Dong, F., Birmili, W., and Wiedensohler, A.: First long-term study of particle number size distributions and new particle for-

mation events of regional aerosol in the North China Plain, Atmos. Chem. Phys., 11, 1565–1580, https://doi.org/10.5194/acp-11-1565-2011, 2011.

Sihto, S.-L., Kulmala, M., Kerminen, V.-M., Dal Maso, M., Petäjä, T., Riipinen, I., Korhonen, H., Arnold, F., Janson, R., Boy, M., Laaksonen, A., and Lehtinen, K. E. J.: Atmospheric sulphuric acid and aerosol formation: implications from atmospheric measurements for nucleation and early growth mechanisms, Atmos. Chem. Phys., 6, 4079–4091, https://doi.org/10.5194/acp-6-4079-2006, 2006.

Vanhanen, J., Mikkilä, J., Lehtipalo, K., Sipilä, M., Manninen, H. E., Siivola, E., Petäjä, T., and Kulmala, M.: Particle Size Magnifier for Nano-CN Detection, Aerosol Sci. Tech., 45, 533–542, https://doi.org/10.1080/02786826.2010.547889, 2011.

Vuollekoski, H., Sihto, S.-L., Kerminen, V.-M., Kulmala, M., and Lehtinen, K. E. J.: A numerical comparison of different methods for determining the particle formation rate, Atmos. Chem. Phys., 12, 2289–2295, https://doi.org/10.5194/acp-12-2289-2012, 2012.

Wang, Z., Wu, Z., Yue, D., Shang, D., Guo, S., Sun, J., Ding, A., Wang, L., Jiang, J., Guo, H., Gao, J., Cheung, H. C., Morawska, L., Keywood, M., and Hu, M.: New particle formation in China: Current knowledge and further directions, Sci. Total Environ., 577, 258–266, https://doi.org/10.1016/j.scitotenv.2016.10.177, 2017.

Wang, Z. B., Hu, M., Yue, D. L., Zheng, J., Zhang, R. Y., Wiedensohler, A., Wu, Z. J., Nieminen, T., and Boy, M.: Evaluation on the role of sulfuric acid in the mechanisms of new particle formation for Beijing case, Atmos. Chem. Phys., 11, 12663–12671, https://doi.org/10.5194/acp-11-12663-2011, 2011.

Wang, Z. B., Hu, M., Sun, J. Y., Wu, Z. J., Yue, D. L., Shen, X. J., Zhang, Y. M., Pei, X. Y., Cheng, Y. F., and Wiedensohler, A.: Characteristics of regional new particle formation in urban and regional background environments in the North China Plain, Atmos. Chem. Phys., 13, 12495–12506, https://doi.org/10.5194/acp-13-12495-2013, 2013.

Wang, Z. B., Hu, M., Pei, X. Y., Zhang, R. Y., Paasonen, P., Zheng, J., Yue, D. L., Wu, Z. J., Boy, M., and Wiedensohler, A.: Connection of organics to atmospheric new particle formation and growth at an urban site of Beijing, Atmos. Environ., 103, 7–17, https://doi.org/10.1016/j.atmosenv.2014.11.069, 2015.

Weber, R. J., Marti, J. J., McMurry, P. H., Eisele, F. L., Tanner, D. J., and Jefferson, A.: Measured atmospheric new particleformation rates: implications for nucleation mechanisms, Chem. Eng. Commun., 151, 53–64, https://doi.org/10.1080/00986449608936541, 1996.

Weber, R. J., Marti, J. J., McMurry, P. H., Eisele, F. L., Tanner, D. J., and Jefferson, A.: Measurements of new particle formation and ultrafine particle growth rates at a clean continental site, J. Geophys. Res.-Atmos., 102, 4375–4385, https://doi.org/10.1029/96jd03656, 1997.

Wu, Z., Hu, M., Liu, S., Wehner, B., Bauer, S., Maßling, A., Wiedensohler, A., Petäjä, T., Dal Maso, M., and Kulmala, M.: New particle formation in Beijing, China: Statistical analysis of a 1-year data set, J. Geophys. Res., 112, D09209, https://doi.org/10.1029/2006jd007406, 2007.

Xiao, S., Wang, M. Y., Yao, L., Kulmala, M., Zhou, B., Yang, X., Chen, J. M., Wang, D. F., Fu, Q. Y., Worsnop, D. R., and Wang, L.: Strong atmospheric new particle formation in winter in urban Shanghai, China, Atmos. Chem. Phys., 15, 1769–1781, https://doi.org/10.5194/acp-15-1769-2015, 2015.

Yue, D., Hu, M., Wu, Z., Wang, Z., Guo, S., Wehner, B., Nowak, A., Achtert, P., Wiedensohler, A., Jung, J., Kim, Y. J., and Liu, S.: Characteristics of aerosol size distributions and new particle formation in the summer in Beijing, J. Geophys. Res., 114, D00G12, https://doi.org/10.1029/2008jd010894, 2009.

Zhou, J., Swietlicki, E., Hansson H. C., and Artaxo P.: Submicrometer aerosol particle size distribution and hygroscopic growth measured in the Amazon rain forest during the wet season, J. Geophys. Res., 107, 8055, https://doi.org/10.1029/2000jd000203, 2002.